Energy Consumption Verification of SPD Smart Window, Controllable According to Solar Radiation in South Korea

Yujin Ko [1], Hyogeun Oh [1], Hiki Hong [2],* and Joonki Min [2],*

[1] Department of Mechanical Engineering, Graduate School of KyungHee University, Yongin 17104, Korea; dbwlsrhdl@khu.ac.kr (Y.K.); ohhyogeun@khu.ac.kr (H.O.)
[2] Department of Mechanical Engineering, KyungHee University, Yongin 17104, Korea
* Correspondence: hhong@khu.ac.kr (H.H.); jkmin@khu.ac.kr (J.M.)

check for updates

Abstract: Between 60% and 70% of the total energy load of a house or office occurs through the exteriors of the building, and in the case of offices, heat loss from windows and doors can approach 40%. A need for glass that can artificially control the transmittance of visible light has therefore emerged. Smart windows with suspended particle device (SPD) film can reduce energy consumption by responding to environmental conditions. To measure the effect of SPD windows on the energy requirements for cooling and heating in Korea, we installed a testbed with SPD windows. With TRNSYS18, the comparison between measurements and simulation has been made in order to validate the simulation model with respect to the modeling of an SPD window. Furthermore, the energy requirements of conventional and SPD-applied windows were compared and analyzed for a standard building that represented an actual office building. When weather for the city of Anseong and a two-speed heat pump were used to verify the simulation, the simulated electricity consumption error compared with the testbed was −1.0% for cooling and −0.9% for heating. The annual electricity consumption error was −0.9%. When TMY2 Seoul weather data were applied to the reference building, the decrease in electricity consumption for cooling in the SPD model compared with the non-SPD model was 29.1% and the increase for heating was 15.8%. Annual electricity consumption decreased by 4.1%.

Keywords: smart window; suspended particle device (SPD); testbed; energy requirement; electricity consumption; solar heat gain coefficient (SHGC); TRNSYS18

1. Introduction

Current trends in green building policy in Korea have strengthened and promoted the roadmap toward mandatory zero-energy buildings for the public sector in 2020 and private buildings in 2025 [1]. In addition, to minimize energy demand from buildings, performance standards of insulation and windows are being reinforced through "Energy Saving Design Standards" to improve the exterior performance of buildings. In particular, from 60% to 70% of the total energy load of a house or office occurs through a building's exterior, and in the case of offices, heat loss from windows and doors can approach 40% [2,3]. Due to the reinforcement of government policies such as "Zero Energy Building Certification" and the Green Building Construction Support Act, installation of awnings is now mandatory [4]. In the case of the existing commercially available external venetian blinds, there is a limit in terms of the exterior design elements of the building, and the quality-certification system for energy performance and maintenance is insufficient, making it difficult to ensure the reliability of consumer awning technology. In addition, structural limitations make it difficult to install awnings on most high-rises due to wind pressure [5].

Research on a method of controlling the transmittance of sunlight through glass rather than installing an external shade has involved depositing metal oxides on glass surfaces using chemical vapor deposition, sputtering, or incorporating a substance exhibiting color/discoloration properties into the composition of glass [6]. However, glass produced by these methods does not include an active control function for sunlight. Instead, it offers passive selective shielding or transmission capabilities for a certain wavelength of light, limiting the ability to satisfy consumer needs [7]. Glass that can overcome these limitations has recently become feasible thanks to thin-film materials with various functions, and research on liquid crystal materials in particular has made substantial progress [8–11]. Smart windows, for example, can change shape, reducing a building's energy consumption, through an optimized response to environmental conditions. Such technology improves user comfort and maximizes environmental performance [12–16].

As a preliminary study in Korea, Min et al. conducted a simulation of a window with suspended particle device (SPD) film, one of several methods recently developed to improve the exterior performance of buildings. The energy performance of SPD and conventional windows was evaluated and compared using virtual models, and trends in cooling and heating loads of SPD windows according to window specifications were analyzed. As a result, when SPD film was applied to clear glass with a U-value of 0.77 W/m^2·K, 30% of cooling energy and 27.8% of heating energy were reduced. However, this study had a limitation in that the target of comparison was clear glass, and real-time SPD control was not applied [17,18]. Ko et al. compared and analyzed cooling and heating energy requirements according to window area ratios and controllable solar heat gain coefficient (SHGC) ranges for SPD windows. As a result, when the window area ratio and SPD's controllable SHGC range were 70% and 0.1–0.55, respectively, percentage decrease of annual energy was up to 16.7%. However, this study had a limitation in that a simulation was performed for a small space without verification [19]. Hong et al. studied the relationship between cooling/heating and lighting loads of buildings according to changes in the SHGC and U-values of SPD windows. There was a limit in that comparison with conventional windows was made [20].

Considerable research is focused on using SPD smart windows to reduce the energy requirements of buildings. However, unlike overseas, where research on SPDs is commonplace, testbed construction, experiments, or simulations in Korea are rare, as is research on windows that can respond to changing solar radiation and control the transmittance of sunlight in real time [21–23]. Therefore, we intended to experimentally evaluate the actual performance and the degree of cooling and heating energy saving effect using SPD film that can be produced in Korea, while also validating the simulation model. In addition, by analyzing the energy percent decrease/increase with the verified simulation for the standard building that represents an actual office, we were able to suggest how much gain and loss occurs when SPD film is applied in Korea and what additional research is required to reduce the loss. This study was intended to serve as the basis for future research on SPD films in Korea. To understand the effects of SPD windows in Korea and validate the simulation model, we therefore installed a testbed with SPD windows in the city of Anseong. Energy requirements for cooling and heating were measured from November 2019 to August 2020. Using TRNSYS18 [24], an energy-simulation program for buildings, the experimental data and the simulation results were compared under the same conditions as the testbed. Verified simulation logic was applied to compare the cooling and heating energy requirements of conventional and SPD windows in a standard office building.

2. Materials and Methods

2.1. Experimental Method

In the Anseong testbed, SPD and conventional windows were installed in two separate spaces. The appearance and specifications of the testbed are provided in Figure 1 and Table 1, respectively. An SPD window was installed on the left side and a non-SPD window on the right. A sketch of the SPD window is provided in Figure 2. SPD has different arrangements depending on whether or not

an electric field is applied. In other words, when electricity does not flow on both sides of the SPD film, particles in the SPD move randomly. As a result, solar radiation is absorbed or scattered, and the window becomes dark blue, reducing light transmittance. On the contrary, when an electric field is applied, particles are arranged in the electric field direction by the electric field formed on both ends of the electrode, making it transparent and increasing the light transmittance. Energy requirements for cooling and heating were measured for the space on the left side at the SPD window and compared and verified with a simulation of the testbed. To determine the energy requirements for heating and cooling, heat-pump power consumption was measured. To verify the simulation of the testbed, outdoor and indoor temperature, humidity, and total horizontal solar irradiation were measured every minute. Appearances and specifications of the measuring instruments are provided in Figure 3 and Table 2, respectively.
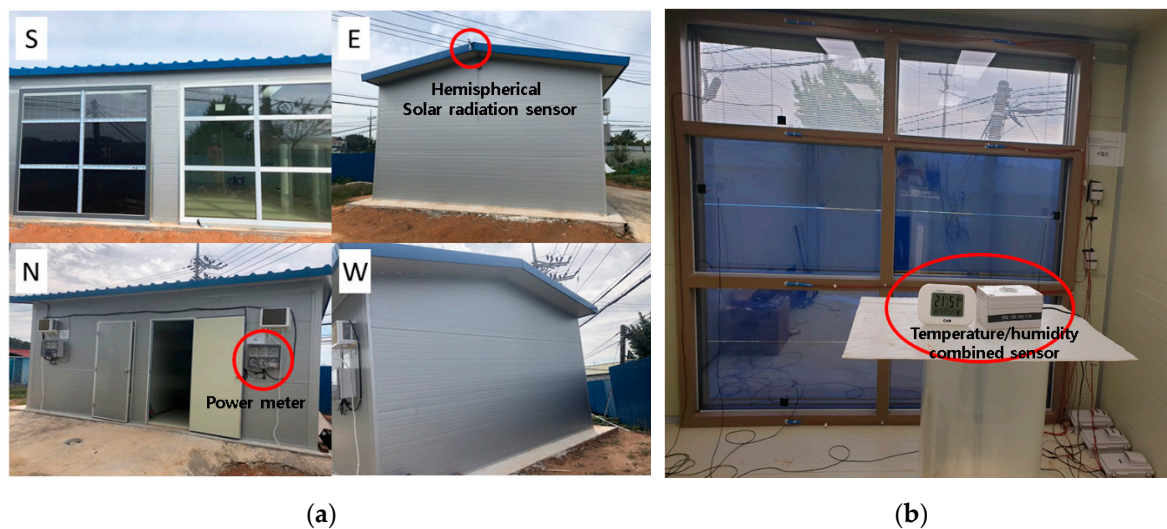
Figure 1. Appearance of testbed in Anseong: (**a**) exterior; (**b**) interior.
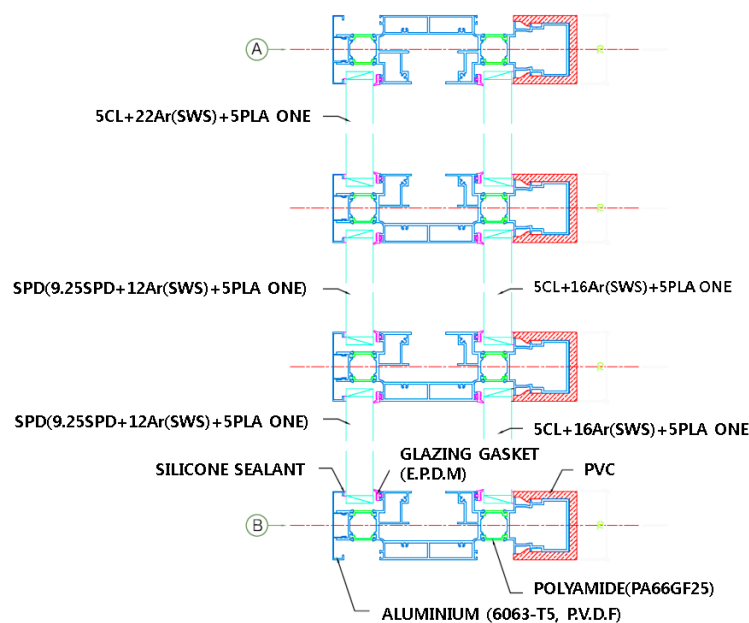
Figure 2. Sketch of the suspended particle device (SPD) window that consist of CL (Clear glass), Ar (SWS, Swiss spacer) and PLA ONE (Planitherm one).

Table 1. Specifications of testbed and simulation input conditions.

Element		Testbed and Simulation	Contents
	Weather data	Anseong	
Size	Floor area	14.57 m^2	
	Number of floors	1	
Shape	Plane	Rectangle	
	Aspect ratio	1.5:1	
	Orientation	South	
	Core	-	
Section	Standard floor height	2.6–3.2 m (2.9 m)	
	Ceiling height	2.445 m	
	Window area ratio	13%	
U-value (W/m^2·K)	External wall	0.401	EPS insulation 100 mm
	Floor/ceiling	0.639	EPS insulation 60 mm
	Roof	0.401	EPS insulation 100 mm
Window	U-value of glazing /glazing + frame	0.47/0.621	SPD9.16 (4CL + 0.38EVA + 0.4SPD + 0.38EVA + 4CL) + 12Ar + 5PLAONE + 114A + 5CL + 16Ar + 5PLAONE
	SHGC	0.11 (Power OFF) ~0.3 (Power max)	Applied real-time SPD control logic according to the amount of solar radiation Controllable SHGC range: 0.19
	Infiltration	1 ACH	
Ventilation	Max	0	
Internal heat	Occupancy	0	
	Light	6 W/m^2	LED
	Equipment	0	
Schedule	Occupancy	08:00–19:00 (Mon. to Fri.)	
	Cooling (Set temperature)	Nov. 2019 (22 °C) Jun. 2020 to Aug. 2020 (24 °C)	
	Heating (Set temperature)	Dec. 2019 to Feb. 2020 (22 °C) Mar. 2020 to May 2020 (24 °C)	

(**a**)　　　　　　　　　　　　(**b**)　　　　　　　　　　　　(**c**)
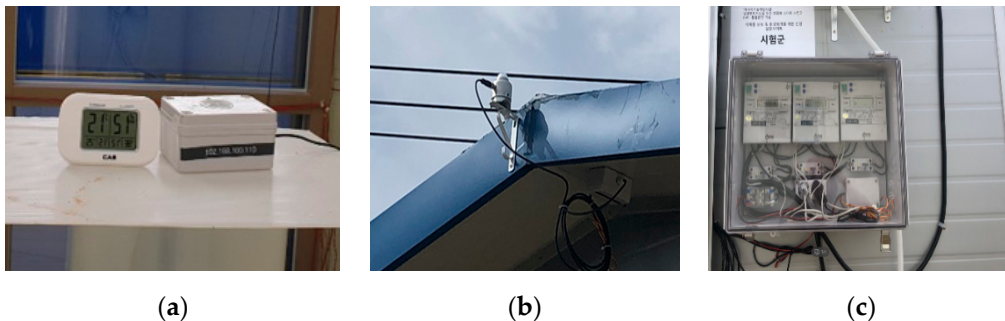
Figure 3. Measuring instruments: (**a**) temperature/humidity combined sensor; (**b**) hemispherical solar radiation sensor; (**c**) power meter.

Table 2. Specifications of measuring instruments.

Type		Product	Accuracy	Resolution	Range	Response Time
Temperature/humidity combined sensor	Temperature	AOSON GAM2320	±0.5 °C	0.1 °C	from −40 to 80 °C	<5 s
	Humidity		±0.3% RH	0.1% RH	max 99.9% RH	<5 s
Hemispherical solar radiation sensor		Hukseflux SR05 series	10% (daily) 20% (hourly)	0.2 W/m^2	from 0 to 2000 W/m^2	18 s
Power sensor		Namjun Co., Ltd. NJ12-210-GEN	±2%	0.2 W	Single phase 2-wire type	

To insulate the buildings, 100 mm of expanded polystyrene (EPS) was installed in the interior walls and roof, and 50 mm of EPS was used for the ceiling and floor. The SPD windows, which were manufactured by Hapdong Hitech Glass Co., Ltd., were double-glazed, and both the exterior and interior panes consisted of double-layered glass. The SPD film was attached only to the exterior pane, the interior pane was composed of conventional glass only, and an air layer was left between them. Table 3 provides the specifications of the double-glazed window before the SPD film was attached.

Table 3. Window (Glazing) specification in testbed without SPD film.

Window	Visible Light (%)		Solar Radiation (%)		SC/ SHGC	U-Value (W/m^2·K)
	Transmittance	Reflectance Exterior/ Interior	Transmittance	Reflectance Exterior/ Interior		KS Winter
CC44.2 (4CL + 0.76PVB + 4CL) + 12Ar + 5PLAONE /114A/ 5CL + 16Ar + 5PLAONE	51	32/34	23	33/47	0.37/0.32 [1]	0.47

[1] After the SPD film is attached, the SHGC is 0.11 with no voltage is applied and refer to Table 1 for specifications after attaching the SPD film.

After the SPD film is attached, the U-value of the window does not change, but both the SHGC and visible light transmittance changes [25]. The SHGC changes according to the voltage applied to the SPD film. In this study, an electrical potential of between 0 and 155 V was applied. In the case of testbed SPD windows, the SHGC was 0.11 in the absence of applied voltage (blocking most of the solar heat). When the applied voltage reached its maximum value, the SHGC was less than that of the window before the SPD film was attached (0.32), showing a controllable range of 0.11 to 0.3. A logic circuit helped keep the applied voltage close to 0.11 when the amount of incoming solar radiation was high and close to 0.3 when the solar radiation was low. At this time, rather than simply fixing it at 0.11 to prevent incoming solar radiation, we tried to minimize the amount of lighting power consumption that can occur by darkening the window by appropriately applying a value between 0.11 and 0.3 in proportion to the difference between reference and the actual incoming solar radiation in real time [26]. The time and the amount of solar radiation flowing into the window were set as input variables and voltage was the output variable. The voltage was applied to the SPD film in real time by comparing real-time solar radiation with reference solar radiation. The room was maintained at comfortable conditions by changing the SHGC value of the window. The control logic was applied only to cooling. During heating, when solar heating is advantageous, the SHGC was fixed at a maximum value of 0.3 (within the controllable range of 0.11 to 0.3). Specifications for the SPD control device are supplied in Table 4.

Table 4. Specification of SPD control device.

Category	Description
Control communication standard	Digital Audio signal (I2S), DAC
Input Voltage	24–48 Vdc
Output Voltage	15 Vdc → 280 Vac
Output Wave	60 Hz Sin-wave
Transformer	from 15 to 280 V
Ext. Driver IF	1 UART port

Table 5 provides the specifications of the heat pump used in the testbed. Power consumption was measured from November 2019 to August 2020. Cooling took place on November 2019 and from June 2020 to August 2020, and heating from December 2019 to May 2020. Power consumption for cooling and heating is shown to compare testbed and simulation data from June 2020 to August 2020 and from December 2019 to March 2020, respectively.

Table 5. Heat-pump specifications installed in the testbed/applied to the simulation.

Parameter		Unit	Value
Heat pump in testbed/heat pump with one-speed operation in simulation	Rated total cooling capacity	W	2500
	Rated cooling power	W	770
	Rated total heating capacity	W	3200
	Rated heating power	W	860
	Rated air flow rate	CMH	1200
Heat pump with two-speed operation in simulation	Rated total cooling capacity (low/high)	W	1388.9/2500
	Rated cooling power (low/high)	W	296/770
	Rated total heating capacity (low/high)	W	1684.2/3200
	Rated heating power (low/high)	W	344/860
	Rated air flow rate	CMH	1200

2.2. Simulation Verification Method

Using TRNSYS18, the experimental data and the simulation results were compared under the same conditions as the testbed. First, the simulation modeling of testbed was performed in SketchUp (Figure 4). Next, the same wall and window conditions as the testbed were applied in TRNBuild [24]. For the control logic that helped change the SHGC of the SPD window according to solar radiation, the shading factor in TRNBuild and the equation component in Simulation Studio were used. The control algorithm for the heat pump was difficult to determine due to the use of an inverter. Simulations therefore implemented single-speed and two-speed operation using Type954c and Type922c components, respectively. This produced a heat-pump control method that reduced the error between the simulation results and the experimental data. In the case of single-speed operation, the specifications for the heat pump in the testbed were applied unchanged, and in the case of two-speed operation, the specifications were applied to "high-speed" among the "low-speed" and "high-speed" options (Table 5). The temperatures for cooling and heating were set to the same values as the testbed, and the heat pump's on/off setting was determined by the room temperature. Simulation input conditions are available in Table 1 along with the testbed conditions.
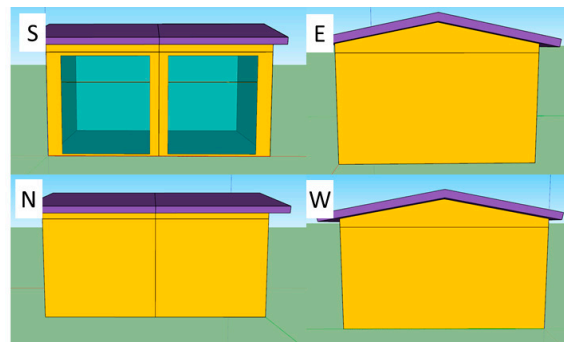
Figure 4. Modeling of testbed.

Meteorological data including outside air temperature, relative humidity, and solar radiation that were measured in the testbed were applied to the simulation using Type 9c. Due to experimental restrictions, weather data were not collected smoothly for several days each month. The simulation exempted these days, and comparisons between simulated and experimental data were limited to days for which experimental data were available. Table 6 supplies the number of days the simulation was conducted per month, and the overall simulation configuration is shown in Figure 5.

Table 6. The number of days the simulation was conducted per month.

Month	11	12	1	2	3	4	5	6	7	8
Days	20	24	25	26	21	23	20	22	23	29
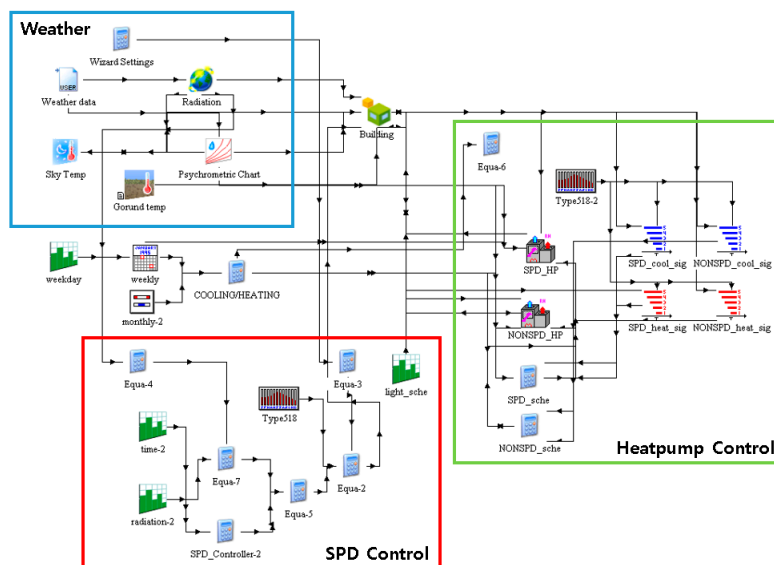
Figure 5. Configuration of testbed simulation.

2.3. Standard Building Simulation Method

The simulation of the standard building that represented an actual office building was based on the verified conditions. Simulations were conducted for two reference buildings with the same conditions, except for those of the window, using both SPD and non-SPD models. The energy requirements for heating and cooling were compared and analyzed for the case in which the SPD film was applied to all existing windows (SPD model) and the case in which the SPD film was not applied (non-SPD model). Figure 6 depicts the SketchUp 3D model and floor plane of the reference building.
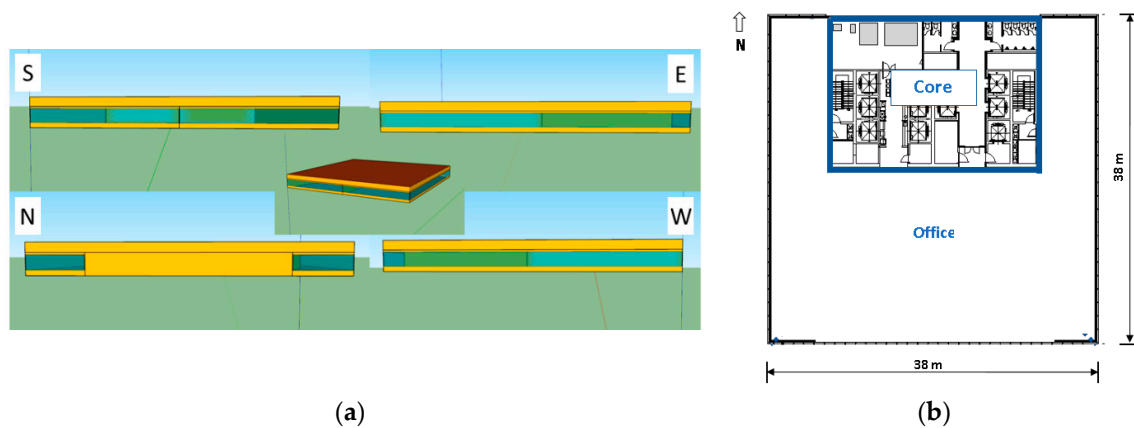
Figure 6. Modeling of standard office building (middle floor only): (**a**) 3D model; (**b**) floor plane.

For the walls of the standard building, U-values and surface resistance were based on the "Energy Saving Design Plan (Notice 2017-881)" [4]. For SPD windows, only double-layered glass with SPD applied to the outside of the double-glazed window in the testbed was used. For the non-SPD window, the SPD film was not attached under the same conditions as the SPD window. In other words, the U-values of SPD and non-SPD windows were the same, but SPD windows differed in that the SHGC value was changed by applying real-time voltage control according to solar radiation. The controllable SHGC range of the SPD model's window was 0.11–0.3 (the same as the testbed), and the SHGC value of the non-SPD model's window without the SPD film was 0.5. The same logic as the previous simulation for testbed verification was used for the SPD control logic. Detailed standard building input conditions are provided in Table 7.

The same Anseong meteorological data as the those applied to the previous testbed simulation and TMY2 (Typical Meteorological Year Data) Seoul weather data embedded in the TRNSYS18 library were used. In both cases, the cooling and heating energy requirements of the SPD and non-SPD models were compared and analyzed. Anseong weather data were measured between November 2019 and August 2020, and TMY2 SEOUL used standard weather data. To derive the energy requirements, the interior of the standard building was divided into four zones, and two different heat-pump capacities were applied to each area. Of the four zones, two had the same area. In the case of the heat pump, two-speed operational component Type922c was used. Table 8 supplies the heat-pump specifications.

Cooling occurred in Anseong on November 2019, and from June 2020 to August 2020, and for TMY2 Seoul from June to November. The set temperature was 26 °C. Heating occurred in Anseong from December 2019 to May 2020 and for TMY2 Seoul from January to March and in December. The set temperature was 18 °C. The heat pump's on/off setting was determined by the room temperature based on the set temperature. When deriving the heat-pump power consumption for cooling, only the period from June 2020 to August 2020 was considered for the Anseong weather data; for TMY2 Seoul, the period from June to September was considered. When deriving the heat-pump power consumption for heating, December 2019 to March 2020 was considered for the Anseong weather data, and January to March and December was considered for TMY2 Seoul. In the case of ventilation, all zones except the core and plenum were ventilated using Type667, a plate-type energy-recovery ventilator component. The effectiveness of the ventilator is described in Table 9, and the standard building simulation configuration is depicted in Figure 7.

Table 7. Input conditions of standard office building simulation.

Element		SPD	Non-SPD
Weather data		Anseong	
		TMY2 Seoul	
Size	Floor area	1444 m^2	
	Number of floors	1 (Middle floor)	
Shape	Plane	Rectangle	
	Aspect ratio	1:01	
	Orientation	South	
	Core	Eccentric (424.8 m^2)	
Section	Standard floor height	3.9 m	
	Ceiling height	2.7 m	
	Window area ratio	38.70%	
U-value (W/m^2·K)	External wall	0.22	
	Floor/ceiling	3.39	
Surface resistance (m^2·K/W)	Wall	Interior: 0.11; Exterior: 0.043	
	Floor/ceiling	Interior: 0.086; Exterior: 0.043	
Window	U-value of glazing /glazing + frame	1.47/1.01	
	SHGC	0.11 (Power OFF) ~0.3 (Power max)	0.5
Infiltration		0.3 ACH	
Ventilation	Max	0.57CMM/person Ventilation control in proportion to the number of occupants	
Internal heat	Occupancy	0.2 person/m^2	
	Light	6 W/m^2	
	Equipment	0	
Schedule	Occupancy	08:00–19:00 (Monday to Friday)	
	Cooling (Set temperature)	Anseong: November 2019, June 2020 to August 2020 (26 °C) TMY2: June to August (26 °C)	
	Heating (Set temperature)	Anseong: December 2019 to May 2020 (18 °C) TMY2: Jan. to May, Dec. (18 °C)	
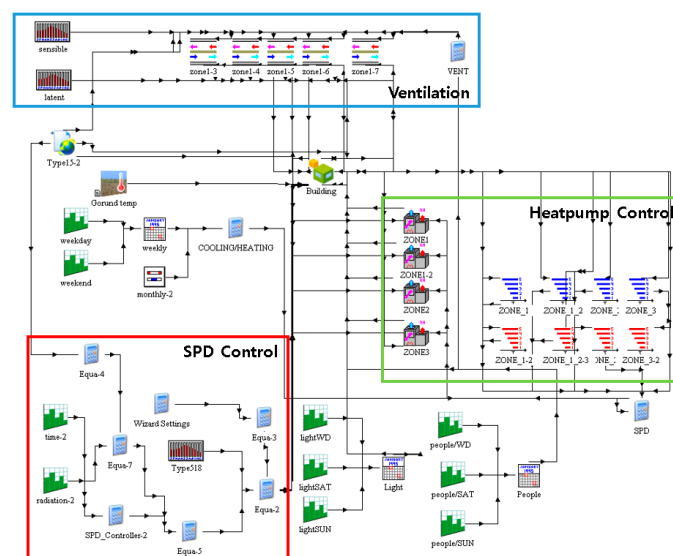
Figure 7. Configuration of standard building simulation.

Table 8. Heat-pump specifications applied to the standard building.

Area	Parameter	Unit	Value
273.9 m^2	Rated total cooling capacity (low/high)	kW	15.0/29.0
	Rated cooling power (low/high)	kW	4.6/11.5
	Rated total heating capacity (low/high)	kW	17.0/33.0
	Rated heating power (low/high)	kW	4.7/12.5
	Rated air flow rate	CMH	4680
	Rated indoor fan power	W	380
	Rated outdoor fan power	W	400
191.4 m^2	Rated total cooling capacity (low/high)	kW	11.0/21.0
	Rated cooling power (low/high)	kW	3.3/7.7
	Rated total heating capacity (low/high)	kW	12.0/24.0
	Rated heating power (low/high)	kW	4.1/7.85
	Rated air flow rate	CMH	3840
	Rated indoor fan power	W	200
	Rated outdoor fan power	W	400

Table 9. Effectiveness of energy recovery ventilation system.

Cooling	Sensible effectiveness	0.7
	Latent effectiveness	0.35
Heating	Sensible effectiveness	0.79
	Latent effectiveness	0.56

3. Results and Discussion

3.1. Comparison Between Experiment and Simulation

To minimize errors between simulation results and experimental data, simulations were conducted for three cases using meteorological data and heat-pump specifications as variables. First, single-speed operation of the heat pump was applied, and because the Meteorological Administration of Korea does not supply solar radiation data for Anseong, data for Suwon (the closest data-collection point) was used [27] (Case 1). Second, single-speed operation of the heat pump was maintained, and meteorological data were replaced with Anseong measured weather data (Case 2). Third, two-speed operation of the heat pump was carried out with Anseong weather data (Case 3).

The results of Case 1 are shown in Figure 8 and listed in Table 10. A monthly comparison of the testbed measured data and the simulation results is shown in Figure 8. Because the percentage errors were not similar for each month, a large difference between them was evident; as errors close to 30% occurred in several months, the simulation cannot be said to represent the experiment. Table 10 provides the cooling, heating, and annual electricity consumption for Case 1. Cooling electricity consumption showed RMSE (Root Mean Square Error) of 18.8%, heating electricity energy consumption showed RMSE of 26.1%, and the difference in annual electricity consumption showed RMSE of approximately 25.0%. The Suwon weather data may not have been appropriate replacements for Anseong data, as the RMSE was large.
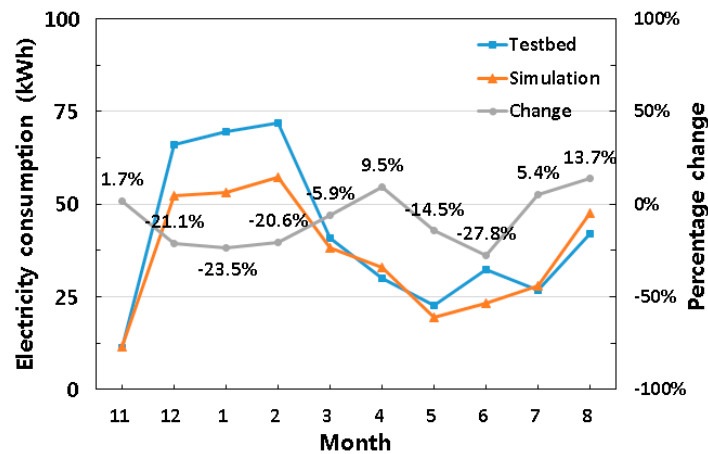
Figure 8. Case 1: Suwon weather data + single-speed operation heat pump.

Table 10. Comparison of heat-pump power consumption (kWh) for cooling/heating of testbed and simulation.

Category		Cooling (kWh)	Heating (kWh)	Total (kWh)
Testbed		101.0	248.3	349.2
Simulation (RMSE)	Case 1	99.2 (18.8%)	200.8 (26.1%)	299.9 (25.0%)
	Case 2	151.5 (39.0%)	183.3 (37.5%)	334.8 (38.2%)
	Case 3	100.0 (11.9%)	246.0 (3.8%)	346.0 (6.4%)

The results of Case 2 are provided in Figure 9 and Table 10. Heating showed a large negative percentage error as in Case 1, but in cooling, the amount of electricity consumed was larger than the experimental data, producing a large positive percentage error. Table 10 shows the cooling, heating, and annual electricity consumption for Case 2. Cooling and heating electricity consumption showed RMSE of 39.0% and 37.5%, respectively. The annual simulation results showed RMSE of approximately 38.2% This was similar to the experimental data in terms of graph trends when simulation results were obtained using measured weather data for Anseong instead of Suwon weather data from the Meteorological Administration of Korea.
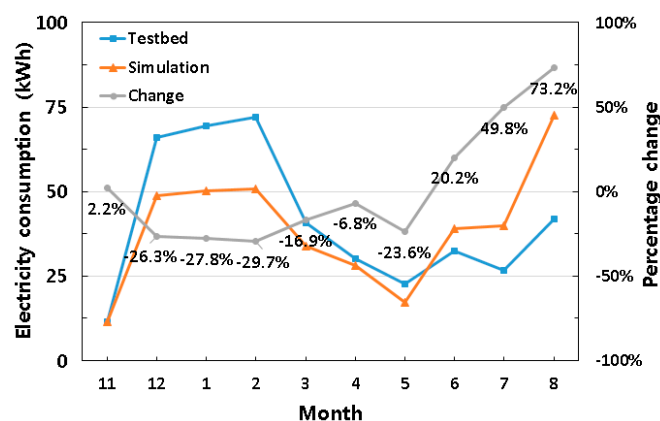
Figure 9. Case 2: Anseong weather data + single-speed operation heat pump.

Results for Case 3 are shown in Figure 10 and Table 10. The graph reveals that the testbed and simulation data nearly overlap, except for in May and June. In May and June, the door was opened often due to entry into the testbed, and electricity consumption in the testbed was higher than that of the simulation. Rather than a single-speed operation heat pump that operates on/off with only one

cooling capacity, it can be seen that the two-speed operation, which operates with two different cooling capacities to keep a room closer to the set temperature, shows similar results to the heat pump installed in the testbed (inverter control method applied). Table 10 provides the cooling, heating, and annual electricity consumption for Case 3. Power consumption for cooling showed RMSE of 11.9% compared with the experiment; for heating, RMSE was 3.8%, and for annual power consumption, the RMSE was 6.4%, all of which are relatively small values (within 10%). These results indicate that the simulation adequately represented the experiment, and the results appear to be valid. An additional simulation was therefore conducted for a reference building that represents an actual office building using the verified simulation.
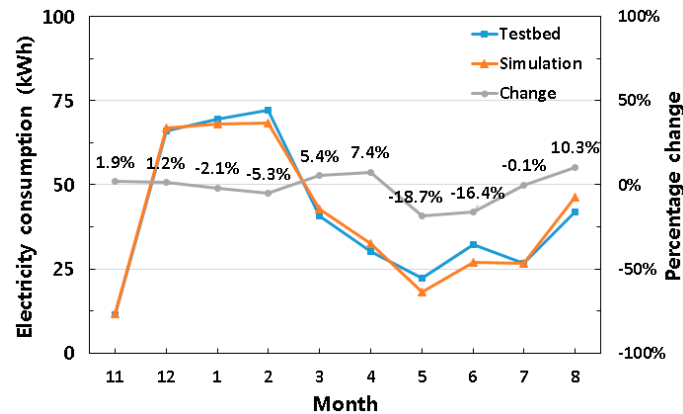
Figure 10. Case 3: Anseong weather data + two-speed operation heat pump.

3.2. Standard Building Simulation

Two simulations were conducted using Anseong and TMY2 Seoul weather data. Results are shown in Figure 11 and Table 11.
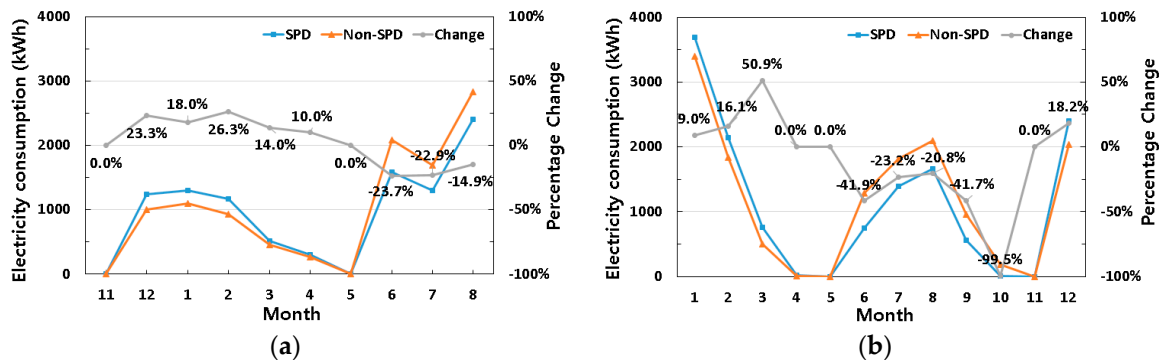
Figure 11. Comparison of heat-pump power consumption between SPD windows and non-SPD windows (standard building): (**a**) measured weather data in Anseong; (**b**) TMY2 Seoul.

Monthly electricity consumption for cooling and heating of the SPD and non-SPD models, using Anseong weather data, is shown in Figure 11a. From December to April, when heating was required, the SPD model consumed more electricity compared with the non-SPD model. In the case of cooling, from June to August, electricity consumption of the SPD model appeared to be lower. Cooling and heating were required in November and May, respectively, but both models showed zero usage as the conditions did not require the heat pump to operate. When the SPD model cooled, and the SHGC of the window was kept between 0.11 and 0.3, the amount of solar heat inflow was smaller than that of non-SPD model, for which the SHGC was fixed at 0.5. This confirmed that the SPD model produced advantageous results while cooling. During heating, the SPD model was fixed at a maximum value of 0.3, but as this value is less than 0.5, inflow of the solar heat through the window

was prevented. The amount of electricity used for heating in the SPD model was therefore higher than that of the non-SPD model. Table 11 provides the cooling, heating, and annual electricity consumption of the two models and the percentage increase/decrease of the SPD model compared with the non-SPD model. In the case of cooling, when SPD windows were used, power consumption decreased by 19.7% compared with the use of non-SPD windows, but heating increased by 21.2%. Because the amount of electricity consumed by cooling was greater than that required for heating, the annual electricity consumption of SPD model decreased by 5.6% compared with the non-SPD model, even though the decrease in cooling was smaller than the increase in heating. It can therefore be assumed that annual energy savings will be greater if applied to areas where summers are harsher than winters.

Table 11. Percent change and cooling/heating electricity consumption of SPD model compared with the non-SPD model (standard building).

Weather Data	Parameter	Model		Cooling	Heating	Total
Anseong		Non-SPD		6605.5	3483.7	10,089.2
		SPD		5301.3	4222.2	9523.5
		Variation		−19.7%	21.2%	−5.6%
TMY2 SEOUL		Non-SPD		6147.7	7768.5	13,916.2
	Standard		SPD	4355.8	8994.2	13,349.9
	(SWEN + 0.11–0.3)		Variation	−29.1%	15.8%	4.1%
	Orientations of windows with SPD applied	SWE	SPD	4477.8	8944.8	13,422.6
			Variation	−27.2%	15.1%	−3.5%
		SEN	SPD	4928	8722.5	13,650.5
			Variation	−19.8%	12.3%	−1.0%
		SWN	SPD	4864.2	8716.9	13,581.1
			Variation	−20.9%	12.2%	−2.4%
	Controllable SHGC range	0.11–0.35	SPD	4467.1	8705.4	13,172.5
			Variation	−27.3%	12.1%	−5.3%
		0.11–0.4	SPD	4577.4	8420.9	12,998.3
			Variation	−25.5%	8.4%	−6.6%
		0.11–0.45	SPD	4688.7	8137.9	12,826.6
			Variation	−23.7%	4.8%	−7.8%

The monthly electricity consumption for cooling and heating in the SPD and non-SPD models, using TMY2 Seoul weather data, is shown in Figure 11b. During heating from January to March and in December, electricity consumption in the SPD model was higher than that in the non-SPD model. In the case of cooling from June to October, electricity consumption of the SPD model appeared to be lower. From April to May and in November, both models showed zero usage as the conditions did not require the heat pump to operate. The graph reveals that the difference in electricity consumption between the two models was larger when cooling than heating. This is confirmed by the data in Table 11 (standard), which shows the cooling, heating, and annual electricity consumption of the two models and the percentage increase/decrease of the SPD model compared with the non-SPD model. In the case of cooling, when SPD windows were used, power consumption decreased by 29.1% compared with the use of non-SPD windows, but heating increased by 15.8%. Unlike the results produced using Anseong data, SPD windows greatly reduced the amount of electricity used for cooling, and the percentage increase in heating was relatively small. Nevertheless, because heating required twice the energy of cooling over the course of a year, the annual decrease in electricity consumption appeared to be only 4.1%, which is less than that of the Anseong case. As such, the effect of using the SPD window during

cooling was about 30%, but the decrease in annual electricity consumption was only approximately 5% because electricity consumption for heating increased simultaneously due to blocking the inflow of solar heat. Further research is therefore needed to reduce the increase in heating energy demand. In this study, the simulation results were confirmed by applying SPD film only to the south, west, and east (SWE); south, west, and north (SWN); and south, east, and north (SEN) orientations, rather than to all four orientations in the SPD model, to examine the trend of the heating energy percentage increase by orientation. In addition, the increase in heating energy appears to be due to the SHGC being controlled at a low value (from 0.11 to 0.3). Expanding this control range from 0.11 to 0.35, from 0.11 to 0.4, and from 0.11 to 0.45, should therefore determine how it affects the increase in heating energy.

3.2.1. Standard Building Simulations According to the Orientation

In the SPD model, the SPD film was applied only to the SWE, SEN, and SWN orientations and the conventional (non-SPD) glass was used for the remaining windows. The differences in electricity consumption between the SPD and non-SPD models are shown in Figure 12. From the graph, it can be seen that the percentage increase in heating energy and the percentage decrease in cooling energy in the order of SWE, SWN, and SEN are both large for all months. Table 11 provides the cooling, heating, and annual electricity consumption percentage changes of the SPD model compared with the non-SPD model. When applied only to a SWE orientation, the cooling energy decreased by 27.2%, the heating energy decreased by 15.1%, and the annual energy decreased by 3.5%. By replacing the north window with a non-SPD type, the amount of solar heat inflow into the building increased, resulting in a decrease in the percentage increase in heating energy by 0.7%p compared with a standard model, but the percentage decrease in cooling energy also fell by 1.4%p. Because the reduction in the percentage decrease of cooling energy was larger, it was disadvantageous in terms of total energy, which fell by 0.6%p compared with the standard model. Next, in the case of the SEN and SWN orientations, which were applied to non-SPD windows to the west and east, compared with the standard model, the cooling energy decrease (19.8% and 20.9%, respectively, compared with the non-SPD model) fell by 9.3%p and 8.2%p, respectively, and the heating energy increase (12.3% and 12.2%, respectively, compared with the non-SPD model) fell by 3.5%p and 3.4%p, respectively. As a result, compared with the standard model, the annual energy decrease for the SEN and SWN orientations fell by 2.2%p and 1.7%p for a decrease of 1.9% and 2.4%, respectively. In both cases, the percentage decrease in cooling energy fell significantly, resulting in a disadvantage in terms of annual energy. However, among the two cases, the SEN orientation, which was applied to non-SPD windows to the west, resulted in lower cooling energy demands and a total energy percentage decrease, indicating that the solar inflow to the west window was larger than east. As a result, replacing the northern window with a non-SPD window to reduce the heating energy increase did not produce a preferred outcome because the heating energy increase did not change significantly, but it was disadvantageous in terms of total energy. In addition, replacing the east or west window with a non-SPD window greatly reduced the beneficial effect of cooling because the inflow of solar radiation from the east and west is large.

(a)

(b)

(c)
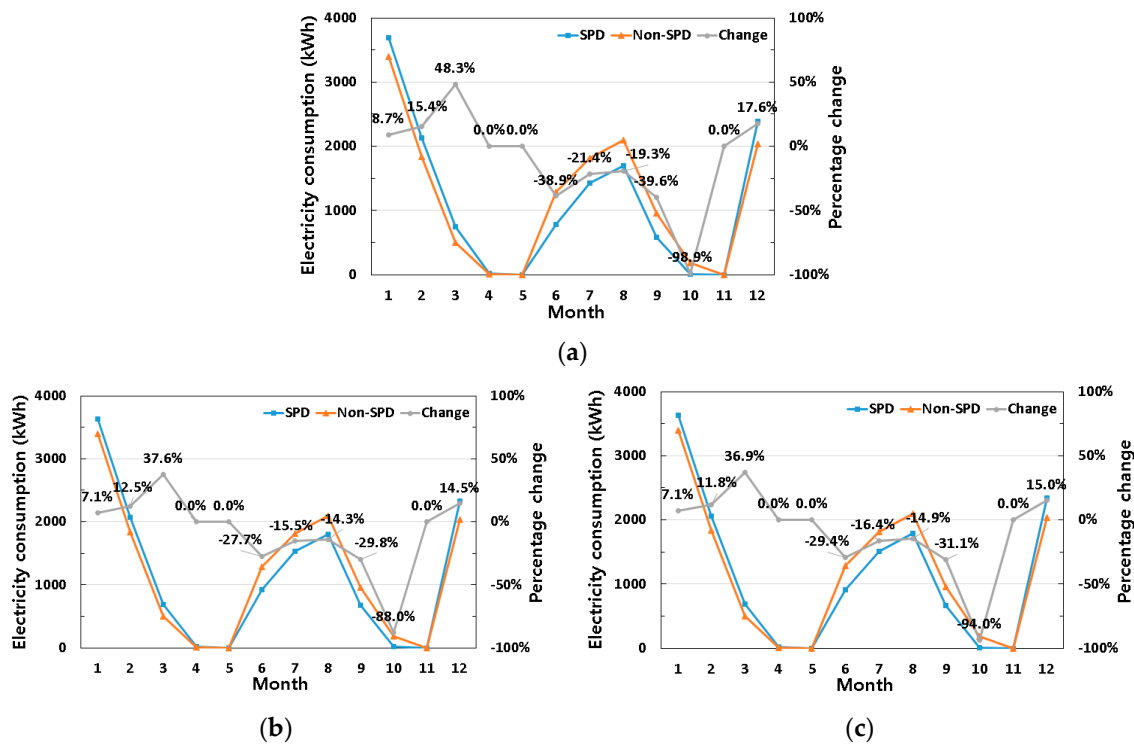
Figure 12. Electricity consumption of SPD/non-SPD models and variation compared to non-SPD model according to the orientation of SPD windows: (**a**) south, west, and east (SWE); (**b**) south, east, and north (SEN); (**c**) south, west, and north (SWN).

3.2.2. Standard Building Simulations According to the Controllable SHGC Range

Figure 13 provides the monthly results of the simulation when changing the controllable SHGC range of the SPD windows to 0.11–0.35, 0.11–0.4, and 0.11–0.45 based on 0.11–0.3. Table 11 shows the cooling, heating, and annual electricity consumption percentage change of the SPD model compared with the non-SPD model. First, when the controllable SHGC range was 0.11–0.35, the cooling energy decrease (27.3%, compared with the non-SPD model) fell by 1.8%p and the heating energy increase (12.1%) fell by 3.7%p compared with the standard model. Because the controllable range of SHGC for SPD windows widened, a higher SHGC value was also distributed more effectively than in the standard model. The amount of solar heat inflow increased and was disadvantageous in cooling. In heating, the maximum value of the controllable SHGC value increased from 0.3 to 0.35, resulting in more favorable results. The percentage decrease in cooling energy decreased, but because the effect of reducing the percentage increase in heating energy was greater, the annual energy decrease rose by 1.2%p compared with the standard (4.1%), resulting in a decrease of 5.3%. Next, in the case of 0.11–0.4 and 0.11–0.45, the cooling energy percentage decrease and the heating energy percentage increase also fell simultaneously. In the case of 0.11–0.4, based on the standard, the cooling energy decrease (25.5%) and the heating energy increase (8.4%) fell by 3.6%p and 7.4%p, respectively. The annual energy decrease was 6.6%, which was 2.5%p higher than the standard (4.1%). In the case of 0.11–0.45, the cooling energy decrease (23.7%) and heating energy increase (4.8%) fell by 5.4%p and 11.0%p, respectively. The annual energy decrease was 7.8%, which was 3.7%p higher than the standard of 4.1%. As the controllable SHGC range increased, the cooling energy percentage decrease of the SPD model fell compared with the standard model, resulting in a disadvantageous cooling result. However, the percentage increase in heating energy also fell, and the decrease was greater than that of cooling. In terms of annual energy, it can be seen that the percentage decrease rose by a factor of approximately 1.9 compared with the standard model. However, because the current SHGC range size was limited to approximately 0.19, research on expanding the range is needed to maximize the effect of SPD.

(a)

(b)

(c)
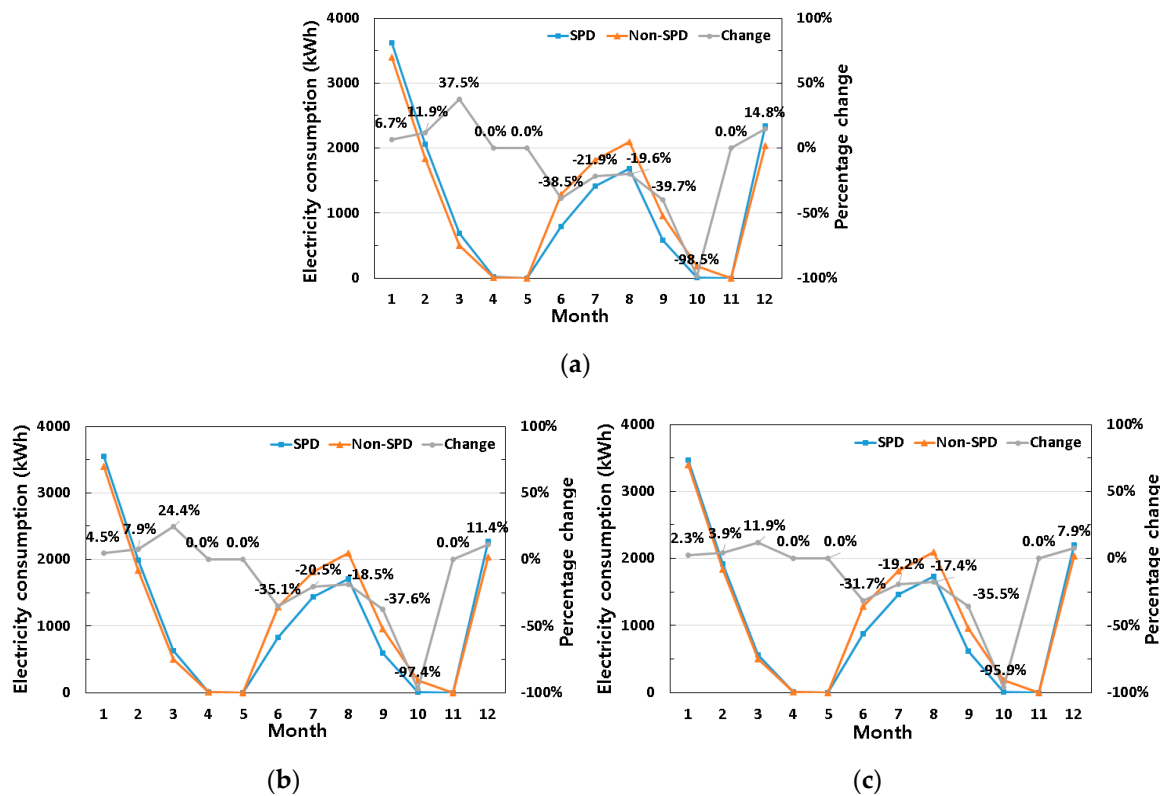
Figure 13. Electricity consumption of SPD/non-SPD models and variation compared to non-SPD model according to the controllable solar heat gain coefficient (SHGC) range: (**a**) 0.11–0.35; (**b**) 0.11–0.4; (**c**) 0.11–0.45.

4. Conclusions

Currently, many efforts are being made to reduce the annual energy consumption in buildings in Korea. This study was conducted to reduce heat loss through windows, which accounts for 40% of the total energy load. Research on smart windows and exactly how much effect and loss occur in real situations in Korea is insufficient. Therefore, through this study, experiment and verification of simulation were conducted. Furthermore, the performance of SPD film was confirmed with respect to the standard building representing an actual office, and comparison with buildings having conventional windows was analyzed. The results were compared by changing the variables that affect energy consumption, and the limitations of the current SPD technology were shown. Through this paper, we aimed to present basic data for future research on SPD film in Korea and to suggest research directions.

Through simulation verification, the error between the measurement and simulation was RMSE 11.9% for cooling, RMSE 3.8% for heating, and RMSE 6.4% for annual energy consumption, showing that the verification was valid. As a result of applying the TMY2 Seoul weather data to the reference building using the verified simulation, the decrease in cooling electricity consumption in the SPD model compared with the non-SPD model was 29.1%, and the increase in heating electricity consumption was 15.8%. The annual electricity consumption decrease was 4.1%. It was confirmed that the percent decrease of cooling energy showed a large value of about 30%, while heating energy increased significantly at the same time. When the SPD film is applied to a conventional window, it has a lower value than the SHGC of original glass, even if it remains the most transparent. Therefore, it is advantageous in terms of cooling, but there are disadvantageous results in heating. Since it is currently technically impossible to expand this SHGC range, the results were compared with two variables through further simulation. First, to reduce the increase in electricity consumption for heating, we attempted to increase the amount of solar heat inflow by applying non-SPD windows to each

orientation, but the results confirmed that the annual electricity consumption percentage decrease fell in all cases. Next, as a result of expanding the controllable SHGC range to reduce the increase in heating electricity consumption, the annual electricity consumption percentage decrease rose by up to a factor of 1.9 as the range widened (controllable SHGC range: 0.11–0.45), and the effect of SPD windows increased. This shows that in order to increase the effect of SPD film, research to expand controllable SHGC range should be conducted.

Author Contributions: Conceptualization, H.H., J.M. and Y.K.; methodology, J.M.; investigation, H.O.; Data Curation, Y.K. and H.O.; writing—original draft preparation, H.H. and Y.K.; and writing—review and editing, J.M. and Y.K. All authors have read and agreed to the published version of the manuscript.

Conflicts of Interest: The authors declare no conflict of interest.

References

1. MOLIT. *Zero Energy Buildung Spread Policy*; Ministry of Land, Infrastructure and Transport: Sejong, Korea, 2019.
2. Najjar, M.K.; Figueiredo, K.; Hammad, A.W.A.; Tam, V.W.Y.; Evangelista, A.C.J.; Haddad, A. A framework to estimate heat energy loss in building operation. *J. Clean. Prod.* **2019**, *235*, 789–800. [CrossRef]
3. Zhao, J.; Du, Y. Multi-objective optimization design for windows and shading configuration considering energy consumption and thermal comfort: A case study for office building in different climatic regions of China. *Sol. Energy* **2020**, *206*, 997–1017. [CrossRef]
4. MOLIT. *Standard of Building Energy Saving*; Ministry of Land, Infrastructure and Transport: Sejong, Korea, 2017.
5. Carletti, C.; Sciurpi, F.; Pierangioli, L.; Asdrubali, F.; Pisello, A.L.; Bianchi, F.; Sambuco, S.; Guattari, C. Thermal and lighting effects of an external venetian blind: Experimental analysis in a full scale test room. *Build. Environ.* **2016**, *106*, 45–56. [CrossRef]
6. Liu, X.; Zhu, J.; Han, J. Numerical and experimental investigation on thermal shock failure of Y2O3-coated CVD ZnS infrared windows. *Int. J. Heat Mass Transf.* **2018**, *124*, 124–130. [CrossRef]
7. Kwak, J.; Kwon, S.W.; Park, S.L.; Yang, J.H.; Lim, K.S. Microcrystalline silicon solar cell using p-a-Si:H window layer deposited by photo-CVD method. *Sol. Energy Mater. Sol. Cells* **2008**, *92*, 1081–1085. [CrossRef]
8. Hemaida, A.; Ghosh, A.; Sundaram, S.; Mallick, T.K. Evaluation of thermal performance for a smart switchable adaptive polymer dispersed liquid crystal (PDLC) glazing. *Sol. Energy* **2020**, *195*, 185–193. [CrossRef]
9. Baetens, R.; Jelle, B.P.; Gustavsen, A. Properties, requirements and possibilities of smart windows for dynamic daylight and solar energy control in buildings: A state-of-the-art review. *Sol. Energy Mater. Sol. Cells* **2010**, *94*, 87–105. [CrossRef]
10. Grnaqvist, C.G. Electrochromics for smart windows: Oxide-based thinfilms and devices. *Thin Solid Film.* **2014**, *564*, 1–38. [CrossRef]
11. Kim, D.-J.; Hwang, D.Y.; Park, J.-Y.; Kim, H.-K. Liquid crystal-Based flexible smart windows on roll-to-roll slot die-Coated Ag nanowire network films. *J. Alloy. Compd.* **2018**, *765*, 1090–1098. [CrossRef]
12. Ghosh, A.; Norton, B. Optimization of PV powered SPD switchable glazing to minimise probability of loss of power supply. *Renew. Energy* **2019**, *131*, 993–1001. [CrossRef]
13. Rezaei, S.D.; Shannigrahi, S.; Ramakrishna, S. A review of conventional, advanced, and smart glazing technologies and materials for improving indoor environment. *Sol. Energy Mater. Sol. Cells* **2017**, *159*, 26–51. [CrossRef]
14. Barrios, D.; Vergaz, R.; Sanches-Pena, J.M.; Garciz-Camara, B.; Granqvist, C.G.; Niklasson, G.A. Simulation of the thickness dependence of the optical propertiesof suspended particle devices. *Sol. Energy Mater. Sol. Cells* **2015**, *143*, 613–622. [CrossRef]
15. Vergaz, R.; Sanchez-Pena, J.M.; Barrios, D.; Vazquez, C.; Contreras-Lallan, P. Modelling and electro-optical testing of suspended particle. *Sol. Energy Mater. Sol. Cells* **2008**, *92*, 1483–1487. [CrossRef]

16. Tallberg, R.; Jelle, B.P.; Loonen, R.; Gao, T.; Hamdy, M. Comparison of the energy saving potential of adaptive and controllable smart windows: A state-of-the-art review and simulation studies of thermochromic, photochromic and electrochromic technologies. *Sol. Energy Mater. Sol. Cells* **2019**, *200*, 109828. [CrossRef]

17. Min, J.; Hong, H. A Study on the Energy Performance Evaluation of a Smart Skin for Reducing Cooling Load of Building Envelope in Office Building. *J. Air-Cond. Refrig. Eng.* **2018**, *30*, 546–557.

18. Min, J.; Ko, Y.; Hong, H. A Study on the Energy Performance Evaluation of Smart Skin for a Test Bed. *J. Air-Cond. Refrig. Eng.* **2019**, *31*, 483–495.

19. Ko, Y.; Hong, H.; Min, J. Energy Performance Evaluation of Responsive Smart Windows Applying SPD According to Window Area Ratio and SHGC Range. *J. Air-Cond. Refrig. Eng.* **2020**, *32*, 441–447.

20. Hong, S.K.; Jang, S.H.; Cho, S.H. A Simulation Study of envelope performance for cooling load reduction in smart envelope system. In Proceeding of the Air-Conditioning and Refrigeration Engineering Winter Conference, Seoul, Korea, 29 November 2017.

21. Ghosh, A.; Norton, B.; Duffy, A. Behavior of a SPD switchable glazing in an outdoor test cell with heat removal under varying weather conditions. *Appl. Energy* **2019**, *180*, 695–706. [CrossRef]

22. Nundy, S.; Ghosh, A. Thermal and visual comfort analysis of adaptive vacuum integrated switchable suspended particle device window for temperate climate. *Renew. Energy* **2020**, *156*, 1361–1372. [CrossRef]

23. Ciampi, G.; Scorpio, M.; Spanodimitrious, Y.; Rosato, A.; Sibilio, S. Thermal model validation of an electric-driven smart window through experimental data and evaluation of the impact on a case study. *Build. Environ.* **2020**, *181*, 107134. [CrossRef]

24. Klein, S.A. *TRNSYS18 Base Manual*; KES Tech: Kocaeli, Turkey, 2019.

25. Research Frontiers. Available online: https://www.smartglass.com/licensees-and-shareholders-of-research-frontiers-get-together-for-introduction-of-highly-energy-efficient-spd-smart-windows/ (accessed on 28 October 2020).

26. Nam, Y.G.; Hong, S.K.; Jang, S.H.; Cho, S.H. A Study on the Effective Control Method of Building Envelope with SPD. In Proceedings of the KSME Autumn Conference, Jeju, Korea, 13 November 2019.

27. KMA. *Suwon Meteorological Data*; Korea Meteorological Administration: Seoul, Korea, 2020.